applied sciences

MDPI

Article

Mechanical Behavior of Steel Fiber-Reinforced Lightweight Concrete Exposed to High Temperatures

Huailiang Wang [1,2], Min Wei [1], Yuhui Wu [1], Jianling Huang [3], Huihua Chen [3] and Baoquan Cheng [3,*]

[1] College of Civil Engineering and Architecture, Guangxi University, Nanning 530004, China; whuailiang@gxu.edu.cn (H.W.); gxuwm@st.gxu.edu.cn (M.W.); gxuwyh@st.gxu.edu.cn (Y.W.)
[2] Key Laboratory of Disaster Prevention and Structural Safety of Ministry of Education, Nanning 530004, China
[3] School of Civil Engineering, Central South University, Changsha 410075, China; hjl1201@csu.edu.cn (J.H.); chh@csu.edu.cn (H.C.)
* Correspondence: 18096562g@connect.polyu.hk

Abstract: The mechanical characteristics of steel fiber-reinforced lightweight concrete (SFLWC) under high temperatures are studied in this paper. Different concrete matrices, including all-lightweight concrete (ALWC) and semi-lightweight concrete (SLWC), and different steel fibers with hooked ends and crimped shapes are considered as objects. In addition, normal-weight limestone aggregates concrete (NWC), no-fiber ALWC, and SLWC were tested after high-temperature treatment as a control group. The temperature effects on the splitting tensile strength, ultrasonic pulse velocity, compressive stress–strain curve, elastic module, peak strain, and axial compressive strength of the SFLWC were investigated. The results showed that, with increasing exposure temperature, both the axial compressive strength and the elastic modulus decreased, while the axial peak strain has a certain increase, and hence the stress–strain curves were gradually flattened. The toughness of all the concretes increased first and then reduced with increasing temperature, while the specific toughness of all the concretes increased with the increase in temperature. Compared with NWC and SLWC, ALWC had a better capacity to resist high temperatures, especially temperatures > 400 °C. Adding steel fibers can improve the capacity of energy absorption, specific toughness, and residual splitting tensile strength of lightweight concrete (LWC) before and after it is exposed to high temperatures. Based on a regression analysis, a segmented constitutive equation for LWC and SFLWC under uniaxial compression was derived from fitting the experimental findings, and the fitting curve agrees well with the test results.

Keywords: steel fiber-reinforced lightweight concrete; mechanical properties; high temperature; constitutive model

Citation: Wang, H.; Wei, M.; Wu, Y.; Huang, J.; Chen, H.; Cheng, B. Mechanical Behavior of Steel Fiber-Reinforced Lightweight Concrete Exposed to High Temperatures. *Appl. Sci.* **2021**, *11*, 116. https://dx.doi.org/10.3390/app11010116

Received: 27 November 2020
Accepted: 21 December 2020
Published: 24 December 2020

1. Introduction

Lightweight concretes (LWC) enjoys the advantages of low density, good sonic and thermal insulation performance, and perfect fire resistance, and have been extensively used as structural and non-structural building materials [1,2]. LWCs can be classified into two types: all-lightweight concretes (ALWCs) and semi-lightweight concretes (SLWCs). For SLWCs, merely coarse lightweight aggregates (LWAs, these can be characterized by porosity, weakness, and brittleness) are employed, while in ALWCs, fine and coarse LWAs are both applied to reduce the self-weight of the LWC structure. Therefore, LWCs have a greater brittleness than normal-weight limestone aggregates concrete (NWC) for similar mix proportions and compressive strength classes [3]. It has been proved that the steel fibers can be added to LWCs to reduce the brittleness of LWC [4,5]. With regard to the influence of steel fibers on the compressive strength of concrete, Dvorkin et al. [6] reported that adding steel fiber with a volume content of 1–1.5% can increase the compressive strength of concrete by 10–25%. Gao et al. [7] showed that adding steel fiber to LWCs increased the compressive strength by 20%. The experimental study by Nicolas et al. [8]

showed that the incorporation of steel fiber increased the compressive strength of the LWC by 60%. However, some studies showed that steel fiber had no significant influence on the compressive strength of LWC [9,10]. Balendran et al. [11] studied the influence of steel fiber with a volume content of 1% on the compressive strength of NWC and high-strength LWC, and the test results showed that steel fiber has little influence on the concrete compressive strength. The negative impact of steel fiber on the compressive strength of LWC has been reported in some references [5,12]. Therefore, it is necessary to enrich the test database with more test results about the influence of steel fiber on the compressive strength of concrete so as to understand the compressive behavior of steel fiber-reinforced lightweight concrete (SFLWC) better. On the other hand, researchers agreed that the incorporation of steel fiber significantly improved the tensile strength, flexural strength, and flexural toughness of LWC [6,7]. According to the existing literature, steel fiber can significantly improve the energy absorption capacity (toughness) of LWC under axial compression [8,13], which is due to the bridging mechanism of steel fiber between cracks in LWC. Studies on the influence of the steel fiber content on the performance of LWC have been quite sufficient. It is worth noting that the addition of steel fiber will reduce the workability of fresh concrete [14], and the slump of fresh LWC will significantly decrease with the increase in the steel fiber volume [15,16]. When the volume admixture is 1.25%, the slump of steel fiber-reinforced high strength self-compacted LWC is lower than the minimum requirement of 600 mm, as reported by Iqbal et al. [17]. For SFLWC with a high content of steel fiber, Li et al. [18] pointed out that when the content of steel fiber was more than 2%, the compactness of SFLWC would be affected. Therefore, a high content of steel fiber will have a negative impact on the workability of fresh SFLWC and the compactness of hardened SFLWC. The high content of steel fiber also increases the unit weight of concrete, which goes against the intention of using light aggregate to reduce the dead load of the structure. On the contrary, steel fibers with too low a dosage may not be useful.

Pająk et al. [19] studied the self-compacting concrete with different types of steel fibers, and the result showed that the improvement of the concrete flexural behavior (toughness and flexural strength) by hooked end steel fiber (HF) was better than that of straight steel fiber. Specimens with HF had a deflection hardening response after the peak point, while the load–deflection curves of specimens with straight fibers were close to those of a plain concrete specimen. Biao et al. [20] studied the influence of different steel fiber types on the flexural behavior of NWC, and the test results showed that HF performed better than crimped shape steel fiber and straight steel fiber. On the other hand, according to Ren et al. [21], the improvement of straight steel fiber on the tensile behavior of ultra-high performance concrete was greater than that of HF, and the improvement of micro straight steel fiber was also greater than that of HF. The above researches indicate that the influence of different types of steel fibers on the mechanical properties of concrete is related to the type of concrete matrix used.

It is well known that the mechanical and physical properties of concrete will degrade to some extent under fire or high temperatures. In extreme cases, post-fire concrete structures without maintenance and retrofitting are no longer suitable to bear any service loading. Existing references show that the type, porosity, and mineral composition of LWA have essential influences on the residual properties of LWC after exposure to high temperatures, and the mineral composition of LWA determines the difference in thermal expansion between cement mortar and aggregate and the development of cracks in the interfacial transition zone [22–26]. As for the influence of steel fiber on concrete after exposure to high temperatures, Khaliq et al. [27] studied the influence of temperature on the mechanical properties of plain NWC and fiber-reinforced NWC. The results showed that the presence of steel fiber improved the residual splitting tensile strength and the elastic modulus of NWC after exposure to high temperatures. According to Zheng et al. [28], the addition of steel fiber significantly improved the residual compressive strength and tensile strength of RPC after exposure to high temperatures. However, there is a lack of research on the residual mechanical performance of LWC and SFLWC exposed to fire and the performance of LWC

containing various steel fiber types under fire. The current work aims to evaluate the effect of steel fiber on the residual mechanical behavior of LWC subjected to fire. Two steel fiber types were applied in this work, including crimped shape steel fiber (CF) and HF. An ALWC matrix with industrial sintered expanded shales as fine and coarse aggregates and a SLWC matrix with sintered fly ash round particles as coarse aggregates were prepared and compared with the NWC. The elastic modulus (stiffness), splitting tensile strength, post-fire compressive strength, compressive toughness, and compressive stress–strain relationship as well as the ultrasonic pulse velocity (UPV) of different mixes were evaluated. Based on the test data, the residual mechanical properties of plain LWC (including ALWC and SLWC) and SFLWC at different temperature levels were expressed as functions of temperature. These series of prediction equations will promote the usage of steel fiber and LWC in fire-resistant applications in the construction industry.

2. Experimental Study

2.1. Raw Materials

Portland cement (P.O. 42.5), according to the Chinese standard (GB175-99) [29], was used for all mixtures. Commercial fly ash and silica fume were applied as an admixture for the LWC and SFLWC. The main physical properties and chemical compositions are presented in Table 1. Crushed limestone (4–20 mm diameter) was used as coarse aggregates of NWC. Crushed shale ceramsite and continuous graded shale ceramsite sand were employed as ALWC coarse and fine aggregates, respectively. Spherical sintered fly ash ceramsite was employed as a SLWC coarse aggregate.

Table 1. Properties of the pozzolanic materials.

Sample	Chemical Composition (%)					Blaine Fineness (cm^2/g)	Density (g/cm^3)	LOI (%)
	SiO_2	Al_2O_3	CaO	Fe_2O_3	MgO			
Cement	21.66	5.42	63.15	2.62	2.89	3110	3.14	1.63
Fly ash	49.10	36.70	4.96	3.67	0.37	3871	2.21	2.08
Silica fume	95.28	0.28	0.35	0.14	0.13	200,000	2.20	1.40

Continuous graded natural river sand was applied as NWC and SLWC fine aggregate. The properties of the aggregates used for the LWCs are presented in Table 2. Two different steel fiber types were used—i.e., hooked end and crimped shape steel fibers. The characteristics of the steel fibers are presented in Table 3. The LWAs and the steel fibers used in the LWC and SFLWC are shown in Figure 1.

Table 2. Properties of the aggregates used for lightweight concretes (LWCs).

Aggregate	Fineness Modulus	Particle Size/(mm)	Apparent Density/(Kg/m^3)	Water Absorption in 24 h/(%)
Crushed shale ceramsite	-	5–20	1390	7.4
Shale ceramsite sand	3.2	≤5	1460	20.8
Sintered fly ash ceramsite	-	4–16	1420	11.3
River sand	2.7	≤5	2670	1.2

Table 3. Characteristics of the steel fibers.

Shape	Length/(mm)	Equivalent Diameter/(mm)	Aspect Ratio	Tensile Strength/(MPa)	Density/(kg/m^3)
Hooked end	35	0.50	70	1200	7800
Crimped	30	0.55	56	800	7800

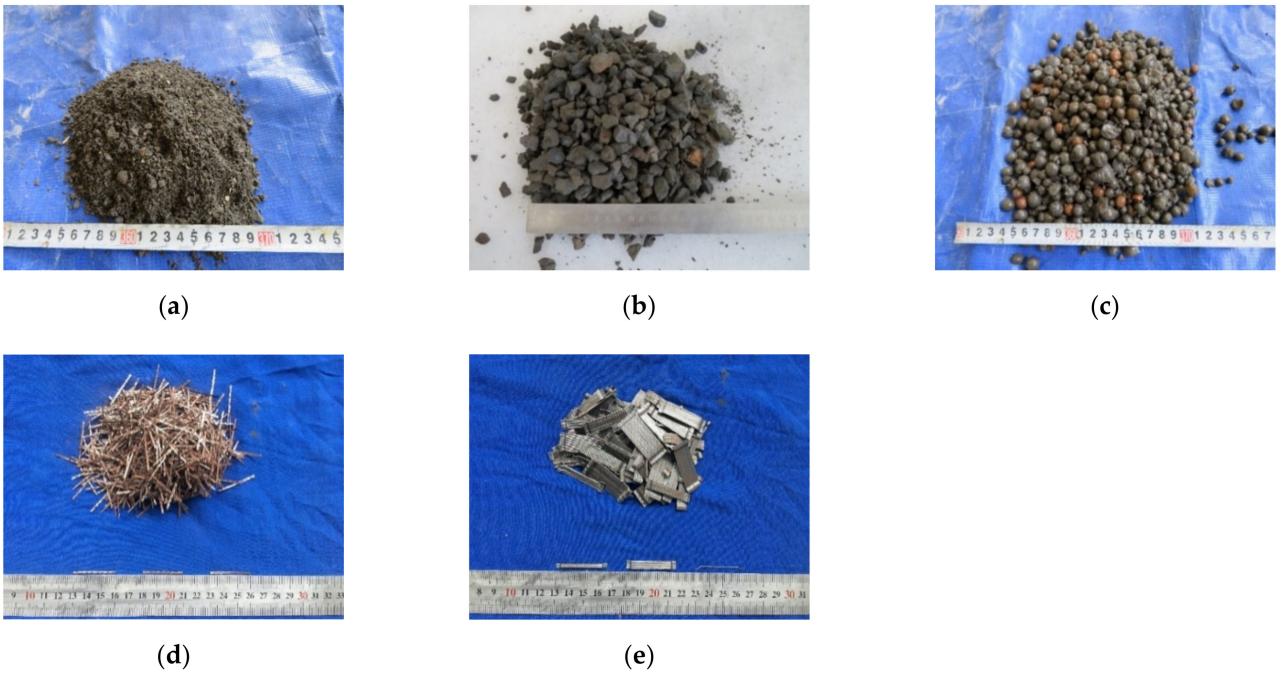

Figure 1. Lightweight aggregates (LWAs) and steel fibers used in the experiment: (**a**) shale ceramsite sand; (**b**) crushed shale ceramsite; (**c**) sintered fly ash ceramsite; (**d**) crimped shape steel fiber; (**e**) hooked end steel fiber.

2.2. Mix Proportioning and Preparation of Test Specimens

Considering the high porosity of LWAs, a large amount of water will be absorbed in the mixing process. Therefore, the crushed shale ceramsite, sintered fly ash ceramsite, and shale ceramsite sand were presoaked for 1 h to achieve a saturated dry surface state for all the LWAs. The total amount of water absorbed by LWAs was calculated, and the effective water binder ratios of SLWC and ALWC were kept at 0.36 and 0.28, respectively. The mixture proportions are listed in Table 4. On this basis, the remaining mixing water, silica fume, fly ash, and cement were mixed for 2 min. Then, the steel fiber was gradually dispersed in the mixture, and the volume fractions of each steel fiber of the concrete mixes in this research were set as 1%. Finally, according to ASTM C143 [30], a superplasticizer (water-reducing admixture) was used for the LWC and SFLWC mixes to achieve workability with slump values of 5–12 cm. After the final mixing for another 5 min to achieve uniformity, steel molds were filled with fresh concrete and vibrated for 60 s. Two kinds of samples were prepared: 100 × 100 × 300 mm prism specimens were employed for axial compressive strength tests and stress–strain curves and 100 × 100 × 100 mm cubic specimens were employed for the UPV and splitting tensile tests. A total of fifteen prisms and fifteen cubes were cast for each mixture proportion, in which three prisms and three cubes were prepared at each temperature. After curing for 24 h, concrete specimens were demolded and stored in the standard curing room for another 28 days at a temperature of 20 ± 2 °C and a relative humidity of 95%.

Table 4. Mixing proportions of the different mixtures (kg/m^3).

Concrete Type	Water	Cement	Silica Fume	Fly Ash	Coarse Aggregate	Fine Aggregate	Super Plasticizer	Steel Fiber
NWC	187	390	-	-	1154	663	-	-
ALWC	154	450	20	80	489	476	8.0	-
CF-AL	154	450	20	80	489	476	8.4	78
HF-AL	154	450	20	80	489	476	8.7	78
SLWC	167	390	14	60	439	821	5.4	-
CF-SL	167	390	14	60	439	821	5.8	78
HF-SL	167	390	14	60	439	821	6.1	78

2.3. Heat Treatment

The test specimens were heated to 200, 400, 600, and 800 °C in an industrial electrical heating furnace type RX-3-45-9. The chamber size of the furnace was 1200 × 600 × 400 mm with a rated power 45kW, rated voltage 380 V, and maximum operating temperature 1000 °C. The heating device is shown in Figure 2a. The heating rate of the furnace was 6 °C/min. Starting from 200 °C, the test samples were heated step by step. The temperature was kept constant for 5 min for each 50 °C. When the target temperature was reached, the temperature was kept constant for 1 h to ensure that both the inside and outside of the samples reached the same target temperature. Then, the furnace was shut down to allow the test samples to cool down naturally to room temperature. After cooling, all the test samples were stored in the laboratory for an additional 7 days before the mechanical properties tests. According to the temperature acquisition system of the resistance furnace, the heating curves of the samples are presented in Figure 2b.

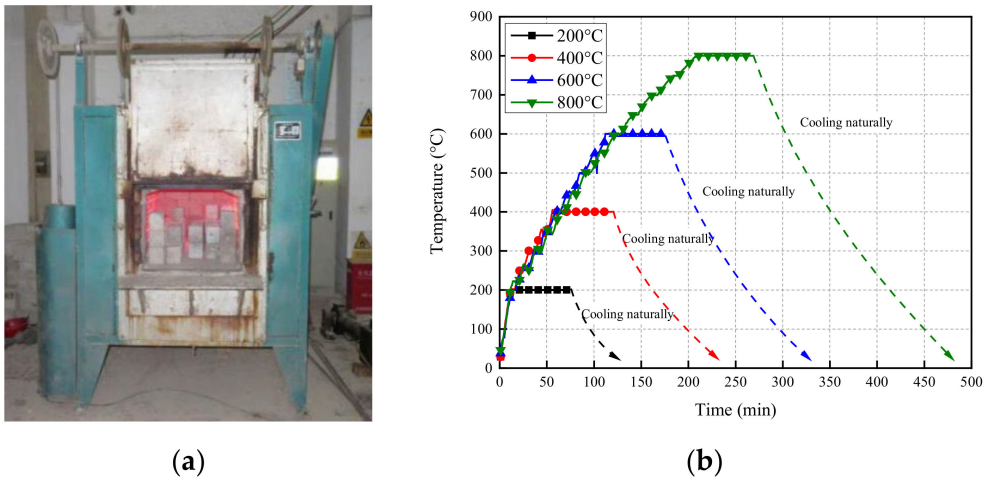

Figure 2. Heat treatment: (**a**) samples in the furnace; (**b**) heating curves of the samples.

2.4. Physical and Mechanical Test

Before the high-temperature test, all the samples were put into the drying oven and dried at 105 °C to reach a constant weight. This serves two purposes: (1) to measure the dry density of all mixtures according to TS EN 12390 [31] and (2) to fully eliminate the influence of free water in the samples during the high-temperature heating process.

Before the mechanical test, the nondestructive test was first conducted on cubic specimens at the ages mentioned above to determine the UPV according to ASTM C597 [32]. After being exposed to each temperature level, the residual UPVs of different mixtures were also measured. Mechanical performance was investigated through splitting tension tests and axial compression tests using the electro-hydraulic servo universal testing machine. A loading rate of 0.8 KN/s was adopted during the splitting tension tests based on the Chinese standard GB/T 50081-2002 [33]. In an axial compression test, two sets of high-precision LVDTs were arranged to record the longitudinal and transverse deformation. Besides this, four concrete strain gauges were glued on the surface of the middle part of the specimen and the longitudinal and transverse strain at the stress–strain curve's ascending section was recorded. The loading process was displacement-controlled. A loading rate of 0.2 mm/min was adopted until the peak load, and the post-peak loading rate was adjusted to 0.08 mm/min until the specimen was destroyed. The above experimental setups are exhibited in Figure 3. The basic physical and mechanical properties of all the concretes (28 d) are listed in Table 5.

(**a**) (**b**) (**c**)

Figure 3. Physical and mechanical tests: (**a**) Ultrasonic pulse velocity (UPV) test; (**b**) splitting tension test; (**c**) axial compression test.

Table 5. Physical and mechanical characteristics of various mixtures at 28 days.

Concrete Type	Oven Dried Density/(kg/m^3)	f_c/MPa	f_{sp}/MPa	UPV/(m/s)	E_c/GPa
NWC	2361	39.36	3.72	4496	28.19
ALWC	1752	48.73	3.33	4016	18.28
CF-AL	1859	49.71	4.17	4090	17.51
HF-AL	1862	51.38	4.73	4098	18.68
SLWC	1888	43.24	3.83	4253	20.25
CF-SL	2007	45.87	4.11	4268	20.27
HF-SL	1954	48.58	4.96	4270	20.43

3. Test Results and Discussions

3.1. Visual and Ultrasonic Inspection of Heated Specimens

The color changes of all kinds of concrete were basically the same after experiencing different heating history: the concrete color was light grey at ambient temperature, while the surface concrete color became dark grey at 200 °C, pink grey or yellow grey at 400 °C, brownish grey at 600 °C and whitish-grey at 800 °C, as presented in Figure 4a. At 200 and 400 °C, there are no significant cracks on the surfaces. However, at 600 °C and 800 °C, there were many irregular cracks on the surface of plain concrete specimens, especially for NWC and SLWC specimens. This may be explained by the different thermal expansion of cement mortar and coarse aggregate. There were a steep temperature gradient and a high internal steam pressure in the specimen at high temperatures. It should be noted that the specimen color does not change significantly, but the number and width of the crack obviously decrease when steel fibers were added. For steel fiber-reinforced ALWC and SLWC specimens, tiny cracks could be observed with naked eyes only after 800 °C. The comparative investigation of the addition of steel fiber is presented in Figure 4b,c. These improvements were due to the fact that steel fibers bridging among cracks can inhibit the developments of cracks [28,34]. Furthermore, the thermal conductivity of steel fiber was higher than plain concrete, making heat transfer more uniform. This helped to reduce the water vapor pressure [35] and the propagation of cracks in the concrete.

Figure 5 presents the relative and absolute values of the residual UPVs of the studied concrete at different elevated temperatures. All the absolute values presented in this study are the average values of the three specimens in each series. The relative value was defined as the ratio between the absolute values obtained after being exposed to high temperatures and room temperature. The same definition of absolute value and relative value are adopted in the following figures. The coefficient of variation of the UPV tests were between 0.2% and 4.2%. It can be observed from Figure 5a that no obvious changes can be observed for ultrasonic pulse velocity when 1% hooked end or crimped steel fiber dosage is added into the concrete. Figure 5b presents the relative residual UPVs of the studied concrete after different elevated temperatures. For all the concrete specimens, the UPV results showed a sudden drop in velocity at 400 °C, which means that the matrix of the concrete experiences considerable damage after exposure to 400 °C. For the NWC and SLWC specimens, the rate

of reduction in UPV values at 400–800 °C was much higher than that at 200 °C. Furthermore, ALWC and steel fiber-reinforced ALWC exhibited the best performance of all the studied concretes. This may be attributed to the similar mineral composition of coarse LWAs and the mortar phase of ALWC, which further led to a more uniform heat transfer and less thermal expansion difference at the aggregate–mortar interface.

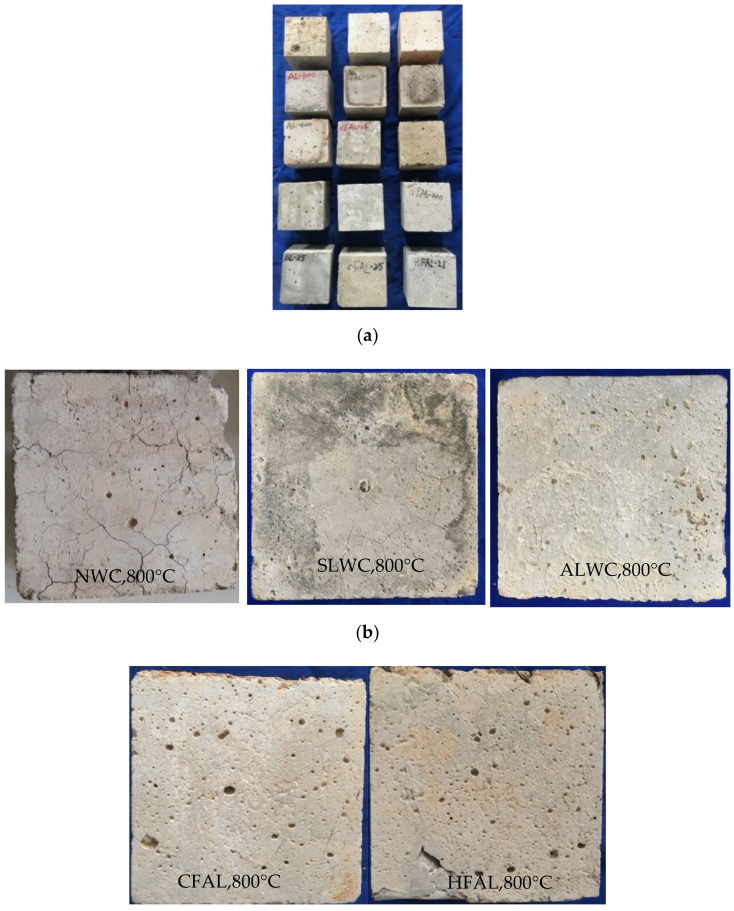

(**a**)

(**b**)

(**c**)

Figure 4. Visual inspection of specimens after exposure to high temperatures: (**a**) the color change of concrete surface after exposure to high temperatures; (**b**) surface cracks of the non-fiber concrete specimen after exposure to 800 °C; (**c**) surface cracks of the added-fiber concrete specimen after exposure to 800 °C.

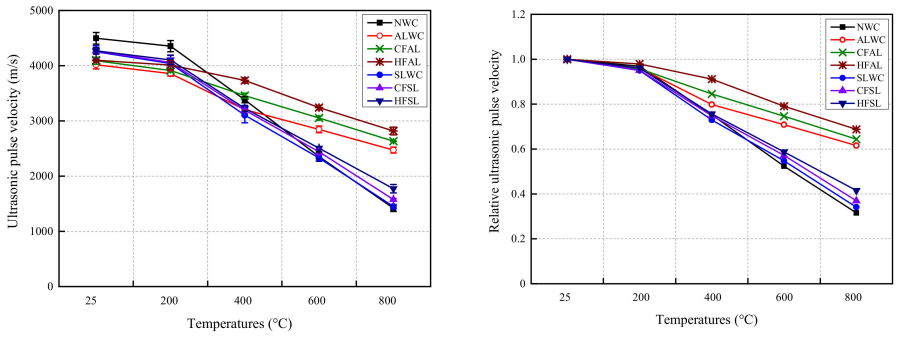

(**a**) (**b**)

Figure 5. Ultrasonic pulse velocities of the studied concrete after the fire: (**a**) absolute UPV; (**b**) relative UPV.

3.2. Splitting Tensile and Axial Compressive Strength

The relative and absolute values of residual axial compressive strength for all the concrete compositions under elevated temperature were plotted in Figure 6. The coefficient of variation of the compression tests were between 0.3% and 12.3%. As shown in Figure 6a, the axial compressive strengths of steel fiber-reinforced LWCs were relatively higher than those of LWC without steel fibers at room temperature. As expected, the decrease in the residual axial compressive strength of all the concrete mixtures was relatively small at 200 and 400 °C, while the strength reduction at temperatures of 600–800 °C was much stronger, as shown in Figure 6b. The strength reduction in the SLWC specimen is similar to that of the NWC test samples under 600 or 800 °C, while the relative residual compressive strength of ALWC was obviously greater than that of SLWC and NWC at about 600–800 °C. This may be because the thermal expansion coefficient of limestone aggregate was greater than LWAs, and limestone dissociates in the temperature range of 600–800 °C due to CaCO3 de-carbonation [36]. Much greater strength loss were observed for SLWC than ALWC. This may be because the bond between the sintered fly ash lightweight aggregates (spherical particle) used in SLWC and the mortar was weakened mainly at high temperatures. The average percentage loss in compressive strength of steel fiber-reinforced ALWC and SLWC were lower than those of LWC without steel fibers after heating at different temperatures. The above research findings agreed with Xie et al. [37], which suggested that steel fiber enhances the compressive and residual strengths at room temperature and elevated temperature, respectively. However, the influence of steel fibers on the relative residual compressive strength of LWC was not as significant as the aggregate types.

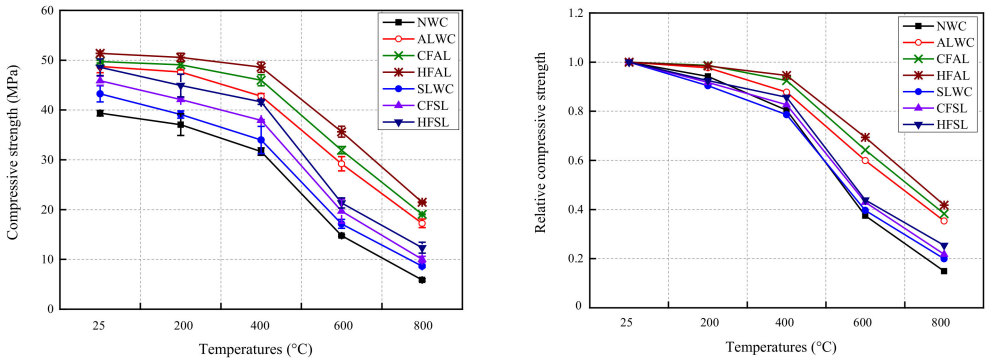

Figure 6. Temperature effect on compressive strength: (**a**) absolute compressive strength; (**b**) relative compressive strength.

The absolute and relative values of the residual splitting tensile strength of all concrete compositions at elevated temperatures are plotted in Figure 7. The coefficient of variation of the splitting tension tests was between 0.7% and 9.1%. Figure 7a shows that the tensile strengths of steel fiber-reinforced LWC are significantly higher than those of LWC without steel fibers at room temperature, which proves the effectiveness of steel fiber in bridging cracks under splitting tensile loading. The enhancement of tensile strengths was more effective for HF types. From Figure 7b, the variation of the residual splitting tensile strength of no fiber concrete specimens was similar to that of the compressive strength. Moreover, it should be mentioned that the tensile strength decay pattern of three concrete batches without steel fiber was almost linear during the temperature range from 200 to 800 °C. It is exciting to find that the splitting tensile strength of LWC with HF suffers less loss than that of LWC with CF in the range of 600–800 °C. It is believed that the bonding strength between LWC matrix and CF reduces sharply at 600 °C, while the reinforcing action of HF drops sharply until 800 °C.

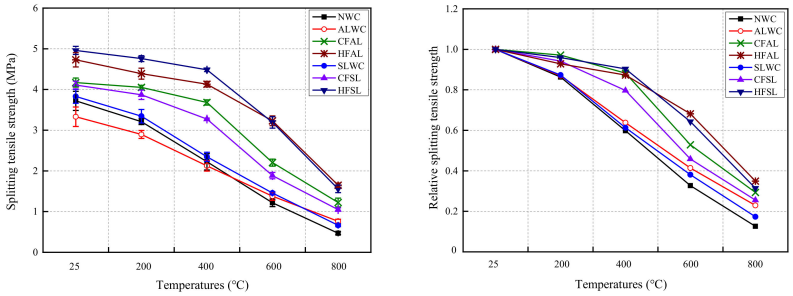

(**a**) (**b**)

Figure 7. Temperature effect on splitting tensile strength: (**a**) absolute splitting tensile strength; (**b**) relative splitting tensile strength.

3.3. Failure Modes after Axial Compression and Compressive Stress–Strain Curves

The failure modes of different concrete mixes after axial compression tests are studied and shown in Figure 8. The transverse deformation of ALWC was larger than that of SLWC and NWC during compression at room temperature. Both the steel fiber types employed in this work significantly helped to improve the toughness of LWC, and more fine cracks appeared on the surface of LWC specimens reinforced with steel fiber during compression. Under similar heat treatments, failure modes and processes of plain LWC specimens with no steel fibers (specimens ALWC and SLWC) were characterized by inclined and tortuous failure planes, while adding steel fiber prevented the overall disintegration of concrete prisms when treated at high temperatures. On the failure surface of heated samples, lightweight aggregates were crushed and many CFs were pulled out. For samples exposed to 600 and 800 °C, HF-reinforced samples had more multiple thinner cracks after compression than CF reinforced samples. Such a phenomenon was attributed to the higher bonding capacity between HF and concrete matrix, which is in accordance with the conclusions that HFs can more effectively reduce the degradation of strength and toughness of concrete under elevated temperatures.

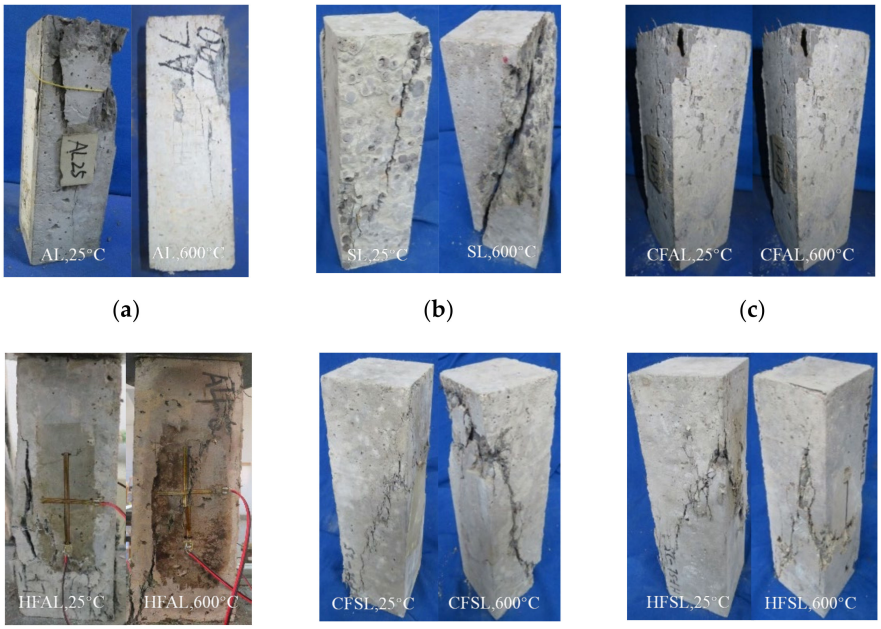

(**a**) (**b**) (**c**)

(**d**) (**e**) (**f**)

Figure 8. Failure mode of mixes after compression: (**a**) All-lightweight concrete (ALWC); (**b**) Semi-lightweight concrete (SLWC); (**c**) All-lightweight concrete with crimped shape steel fiber (CFAL); (**d**) All-lightweight concrete with Hooked end steel fiber (HFAL); (**e**) Semi-lightweight concrete with crimped shape steel fiber (CFSL); (**f**) Semi-lightweight concrete with hooked end steel fiber (HFSL).

Figure 9 presents the typical compressive stress–strain curves for different concrete mixtures under different high temperatures. Each set of curves included the axial stress-axial strain and corresponding axial stress–transverse strain curves. Figure 9 shows that the axial peak strain and transverse deformation of LWC are significantly higher than those of NWC at room temperature. Han et al. [38] found that higher volume contents of lightweight aggregate in LWC resulted in longer linear ascending branches of the stress–axial strain curve and a steeper descending section, which means that the brittleness would increase with a decreasing concrete mixture density. Test results prove that LWC was more brittle than NWC of the same strength grade. Compared with SWLC, the stress–strain curve of ALWC was smoother in the ascending section, while it was steeper in the descending section, with relatively larger axial and transverse peak strain. This denoted that ALWC was more brittle than SLWC. The shapes of stress–strain diagrams up to 200 °C were similar to those obtained at room temperature. From 400 to 800 °C, the peak strain increased with increasing temperature, but the peak stress showed a decreasing trend, with a gradually decreasing slope. As a result, the stress–strain curves of all concrete gradually leveled off. Above 400 °C, the loss of strength and stiffness for NWC samples became much greater than those of SLWC and ALWC, and the area under the descending part of the stress–strain curves also decreased more sharply than that of SLWC and ALWC. By adding steel fiber, the peak stress and strain of the ascending curve increased slightly, and the area under the stress–strain curves also increased in the 25–800 °C temperature range. The above results showed that both steel fiber types could enhance the compressive energy absorption capacity of the LWC before and after being exposed to high temperatures. Obviously, the HFs could improve the energy absorption capacity of LWC more effectively.

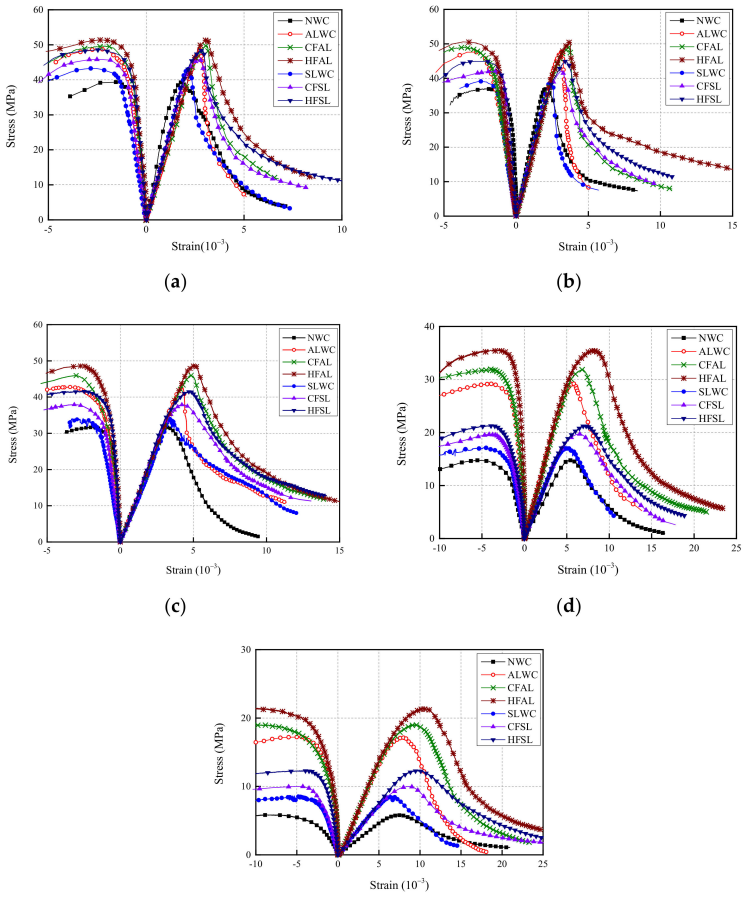

Figure 9. Stress–axial strain curves of all mixes exposed to elevated temperatures: (**a**) 25 °C; (**b**) 200 °C; (**c**) 400 °C; (**d**) 600 °C; (**e**) 800 °C.

3.4. Elastic Modulus and Compressive Peak Strains

The absolute and relative values of residual elastic modulus of all mixtures under elevated temperatures are plotted in Figure 10. According to [39,40], the elasticity modulus of each mixture is determined to be the secant modulus at one third of peak stress on the rising section of the corresponding uniaxial compressive stress–strain curve. The coefficient of variation of the elastic modulus tests was between 5.1% and 22.3%. However, the coefficient of variation of the tests were mostly less than 15%. From Figure 10a, before 400 °C, the elastic modulus of LWC was obviously smaller than that of NWC, and the elastic modulus of ALWC was smaller than that of SLWC. Additionally, the influence of steel fiber on the LWC elastic modulus was relatively small. It assumed that under only 1/3 of the peak load the micro-cracks were not well-developed, and the steel fiber stress was relatively small. Therefore, the characteristics of high elastic modulus and high tensile strength of steel fiber had not been fully developed.

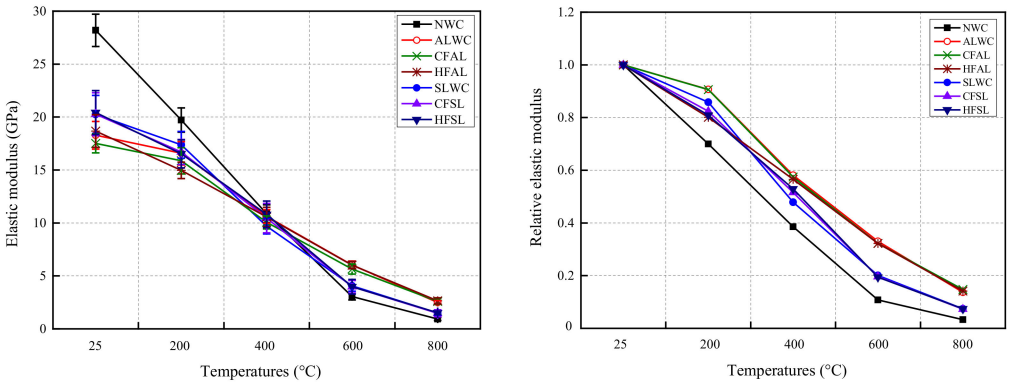

Figure 10. Temperature effect on the elastic modulus: (**a**) absolute elastic modulus; (**b**) relative elastic modulus.

Figure 10b shows that: (1) with increasing temperature, the decrease in the elastic modulus of all mixtures was higher than that of compressive strength. This was because cracks propagate on the interface between cement mortar and coarse aggregate, resulting in loose internal structure, large deformation at high temperature, and a sharp decrease in stiffness at 400, 600 and 800 °C; (2) in the temperature range 200–800 °C, the stiffness loss of NWC was greater than that of LWC, including ALWC and SLWC. In the range of 400–800 °C, the stiffness loss of SLWC is greater than that of ALWC. The above phenomena can be explained by the bond between the aggregate and the mortar, the mineral composition of coarse aggregate, and cement mortar composition of different concrete mixtures. LWAs were prepared by high-temperature calcination and due to the hard enamel "shell" and high internal porosity of the particles, the thermal conductivity and thermal expansion coefficient were low. Therefore, these results led to better fire resistance, and less post-fire stiffness loss than that of NWC [28]. As for the ALWC, due to the same mineral composition of coarse and fine aggregate, the thermal compatibility of the coarse aggregate phase and cement mortar phase was better than that of NWC and SLWC. In addition, compared to the crushed shale ceramist's irregular appearance, the sintered fly ash ceramsite used in SLWC was spherical, which led to the weaker adhesion between coarse aggregate and cement mortar in SLWC. For the above reasons, the stiffness loss of ALWC after the high temperature was less than that of NWC and SLWC.

The absolute and relative values of compressive peak strains of all mixtures under elevated temperatures are plotted in Figure 11. The coefficient of variation of the compressive peak strain tests were between 1.5% and 8.0%. In Figure 11a, the average peak strain of the ALWC measured at room temperature was 2720 με. Compared to that without fibers, when adding CF the corresponding strain of peak stress increased by 12.5%, and when

adding HF the corresponding strain of peak stress increased by 14.7%. The average peak strain of SLWC was 2140 με. Compared to that without fibers, the corresponding strain of peak stress increased by 28.5% with CF, while the corresponding strain of the peak stress increased by 32.7% with HF. For the same LWC matrix, HF had a significant influence on the peak compressive strain. In Figure 11b, the peak strain of the concretes with or without fibers increases gradually with the rise in temperature. Adding steel fiber did not influence the peak strain trend with temperature. The peak strain increment of all mixes was small at 200 °C, but it increased significantly at 400, 600, and 800 °C. The increase in peak strain was due to the inconsistency of thermal expansion between the aggregate and the cement mortar at high temperatures. Due to the lower thermal conductivity and thermal expansion coefficient of LWAs in LWC, the increasing amplitude of the peak compressive strain of ALWC and SLWC with the elevated temperature was smaller than that of NWC.

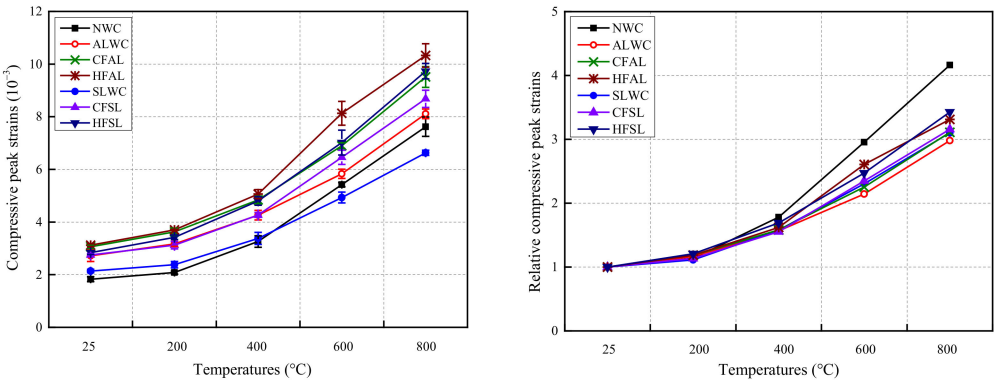

Figure 11. Temperature effect on compressive peak strains: (**a**) absolute compressive peak strains; (**b**) relative compressive peak strains.

3.5. Energy Absorption Capacity (Toughness)

In the current work, the stress–strain curves for concrete were recorded until the load was decreased to one third of the peak load (i.e., $0.33f_{c0}$ of the descending branch, known as "$0.33f_{c0}$ point"), and the concrete energy absorption capacity (toughness) under uniaxial compression was determined based on the area under stress–strain curve before the $0.33f_{c0}$ point. Figure 12 shows the toughness test results under different temperatures. The coefficient of variation of the tests was generally less than 15%. and for some cases the coefficient was slightly higher than 15%. However, for all cases the coefficient of variation was less than 20.6%. Figure 12 demonstrating the energy absorption capacity of NWC was higher than LWC at room temperature. After adding steel fiber, the energy absorption capacity of the LWC is enhanced, and the toughness improvement of LWC by adding HF was the most significant. With the temperature increase, the energy absorption capacity of all the concrete increased first and then decreased. All the concrete samples reached the correspondingly most massive energy absorption capacity at a temperature of 400 °C, except for HFAL. By comparing the data given in Figure 12, it can also be found that, after exposure temperature at 800 °C, the energy absorption capacity of the SLWC and NWC, respectively, decreased to 45.5% and 67.7% compared to that at room temperature. In contrast, the energy absorption capacity of ALWC was 40% higher than that at room temperature. The corresponding percentages for the SLWC reinforced by CF and HF were 71.4% and 83.3%, respectively, while those for the ALWC reinforced by CF and HF were 135.7% and 126.3%, respectively. The above phenomenon shows that the concrete residual energy absorption capacity under high temperatures was primarily related to the aggregate type.

Specific toughness is defined as the ratio of toughness to the compressive strength of the same specimen. Comparing the data given in Figure 13, the coefficient of variation of

the tests was between 0.8% and 20.7%. However, the coefficient of variation of the tests was mostly less than 15%. It can be found that the presence of steel fibers increased the specific toughness in the range of 25 to 800 °C. Furthermore, the specific toughness was enhanced as the temperature increased. It must be noted that the increase in the specific toughness of LWCs was greater than that of NWC. For example, the specific toughness of ALWC was 3.17 and 3.96 times at 600 and 800 °C of that at room temperature, SLWC was 3.08 and 3.34 times, and NWC was 2.42 and 3.06 times, respectively. This was mainly because the concrete strength degradation rate was greater than the toughness degradation rate in the evaluated temperature range.

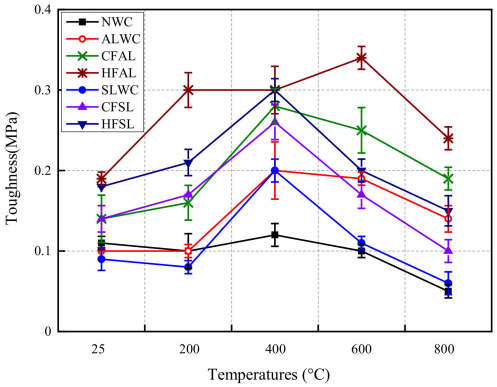

Figure 12. Effect of temperatures on the toughness of different concretes.

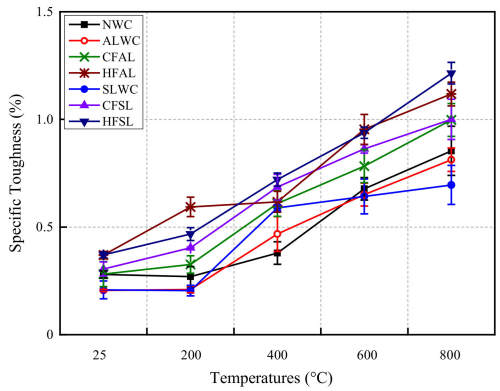

Figure 13. Effect of temperature on the specific toughness of different concretes.

4. Numerical Models

4.1. High-Temperature Property Relationships

Based on the test data of the NWC, LWC, and SFLWC residual mechanical properties in the temperature range of 25–800 °C, the empirical relationships between the mechanical characteristics, including the elasticity modulus, tensile strength, compressive strength, peak strain, and exposed temperature grade, are established. The coefficient β is defined as the ratio of the residual mechanical property index after being exposed to high temperatures to the mechanical property index at room temperature.

$$\beta_c = \frac{f_{c,T}}{f_{c,25}}, \beta_t = \frac{f_{sp,T}}{f_{sp,25}}, \beta_e = \frac{E_{c,T}}{E_{c,25}}, \beta_p = \frac{\varepsilon_{p,T}}{\varepsilon_{p,25}}. \quad (1)$$

The expressions of the compressive strength reduction factor (β_c), splitting tensile strength reduction factor (β_t), elastic modulus reduction factor (β_e), and peak compressive strain amplification factor (β_p) of the NWC, LWC, and SFLWC are derived and given in Table 6. It is noted that when similar β values are inferred from different concrete types, the unified expressions are given.

Table 6. High-temperature property relationships of different mixes.

Property	Relation	Concrete Type
Compressive strength	$\beta_c = \begin{cases} 1.0 & 25\ ^\circ\mathrm{C} \\ -0.959\left(\frac{T}{1000}\right)^2 - 0.293\left(\frac{T}{1000}\right) + 1.020 & 200\ ^\circ\mathrm{C} \le T \le 800\ ^\circ\mathrm{C} \end{cases}$	NWC SL CFSL HFSL (R^2 = 0.96)
	$\beta_c = \begin{cases} 1.0 & 25\ ^\circ\mathrm{C} \\ -1.248\left(\frac{T}{1000}\right)^2 + 0.219\left(\frac{T}{1000}\right) + 0.997 & 200\ ^\circ\mathrm{C} \le T \le 800\ ^\circ\mathrm{C} \end{cases}$	AL CFAL HFAL (R^2 = 0.98)
Splitting tensile strength	$\beta_t = \begin{cases} 1.0 & 25\ ^\circ\mathrm{C} \\ -0.113\left(\frac{T}{1000}\right)^2 - 1.007\left(\frac{T}{1000}\right) + 1.042 & 200\ ^\circ\mathrm{C} \le T \le 800\ ^\circ\mathrm{C} \end{cases}$	NWC AL SL (R^2 = 0.99)
	$\beta_t = \begin{cases} 1.0 & 25\ ^\circ\mathrm{C} \\ -1.008\left(\frac{T}{1000}\right)^2 - 0.156\left(\frac{T}{1000}\right) + 1.018 & 200\ ^\circ\mathrm{C} \le T \le 800\ ^\circ\mathrm{C} \end{cases}$	CFAL CFSL (R^2 = 0.96)
	$\beta_t = \begin{cases} 1.0 & 25\ ^\circ\mathrm{C} \\ -1.318\left(\frac{T}{1000}\right)^2 + 0.252\left(\frac{T}{1000}\right) + 0.980 & 200\ ^\circ\mathrm{C} \le T \le 800\ ^\circ\mathrm{C} \end{cases}$	HFAL HFSL (R^2 = 0.99)
Elastic modulus	$\beta_e = \begin{cases} 1.0 & 25\ ^\circ\mathrm{C} \\ 1.075\left(\frac{T}{1000}\right)^2 - 2.177\left(\frac{T}{1000}\right) + 1.069 & 200\ ^\circ\mathrm{C} \le T \le 800\ ^\circ\mathrm{C} \end{cases}$	NWC (R^2 = 0.99)
	$\beta_e = \begin{cases} 1.0 & 25\ ^\circ\mathrm{C} \\ 0.021\left(\frac{T}{1000}\right)^2 - 1.179\left(\frac{T}{1000}\right) + 1.055 & 200\ ^\circ\mathrm{C} \le T \le 800\ ^\circ\mathrm{C} \end{cases}$	AL CFAL HFAL (R^2 = 0.98)
	$\beta_e = \begin{cases} 1.0 & 25\ ^\circ\mathrm{C} \\ 0.353\left(\frac{T}{1000}\right)^2 - 1.566\left(\frac{T}{1000}\right) + 1.071 & 200\ ^\circ\mathrm{C} \le T \le 800\ ^\circ\mathrm{C} \end{cases}$	SL CFSL HFSL (R^2 = 0.98)
Compressive peak strains	$\beta_p = \begin{cases} 1.0 & 25\ ^\circ\mathrm{C} \\ 4.694\left(\frac{T}{1000}\right)^2 + 0.332\left(\frac{T}{1000}\right) + 0.946 & 200\ ^\circ\mathrm{C} \le T \le 800\ ^\circ\mathrm{C} \end{cases}$	NWC (R^2 = 0.99)
	$\beta_p = \begin{cases} 1.0 & 25\ ^\circ\mathrm{C} \\ 2.873\left(\frac{T}{1000}\right)^2 + 0.491\left(\frac{T}{1000}\right) + 0.971 & 200\ ^\circ\mathrm{C} \le T \le 800\ ^\circ\mathrm{C} \end{cases}$	AL SL CFAL CFSL HFAL HFSL (R^2 = 0.98)

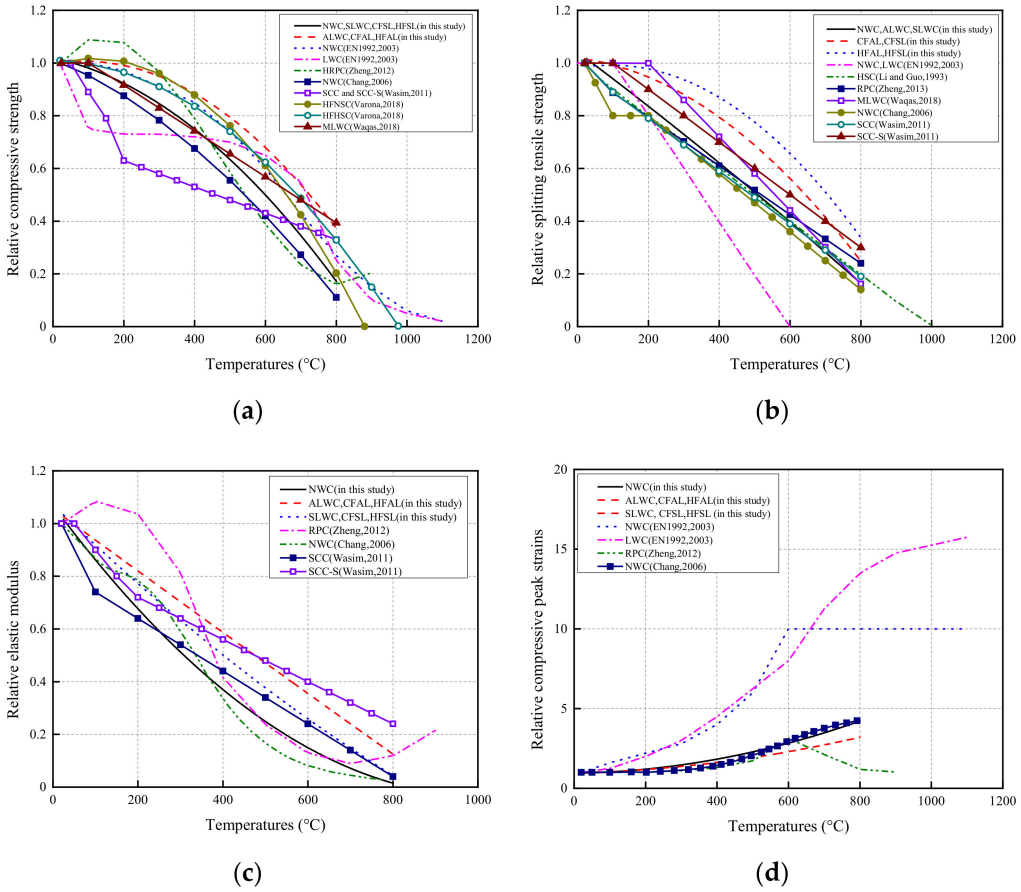

Figure 14. Evolution of the residual mechanical characteristics under high temperatures: (**a**) compressive strength; (**b**) splitting tensile strength; (**c**) elastic modulus; (**d**) compressive peak strains.

Figure 14b also presents the relative residual splitting tensile strength curves of high-strength concrete (HSC), steel fiber-reinforced reactive powder concrete (RPC) [28], MLWC [40], plain and steel fiber-reinforced self-consolidating concretes (SCC and SCC-S), the NWC, and the normalized residual splitting tensile strength given in Euro code 2 (2003) [41]. As presented in Figure 14b, the relative values of splitting tensile strength of concretes without steel fiber (including NWC, SLWC, and ALWC), at each corresponding temperature were close to those of NWC [39], RPC with straight steel fiber [28], and plain SCC [27]. The normalized residual splitting tensile strength after the high temperature was related to the type of steel fiber, and the hook ended steel fiber was more effective in enhancing the relative residual splitting tensile strength of LWC exposed to high temperature. Figure 14c shows the test results of relative residual elastic moduli of NWC, steel fiber-reinforced RPC, SCC, and SCC-S. It is observed that the residual elastic modulus change rule was mainly related to the aggregate type. Adding steel fiber had no obvious influence on the relative residual elastic modulus. Figure 14d presents the relative residual compressive peak strain curves of the NWC, steel fiber-reinforced RPC [42], and the normalized residual compressive peak strains of NWC and LWC given in EN code (2003) [41]. Figure 14d shows that the normalized residual peak compressive strain of NWC exposed to high temperature in this study is basically the same as that of NWC in the literature [39].

4.2. Equation of the Compressive Stress–Strain Curve

At present, there are many mathematical models used to describe the whole stress–strain curves of fiber-reinforced concrete and LWC at room temperature; however, there are few mathematical models to describe the uniaxial constitutive relationships of SFLWC at room temperature. There is no compressive constitutive model of LWC and SFLWC under high temperatures. The stress–strain curves of different concretes before and after high

temperatures are different; hence, different mathematical models are needed to simulate the constitutive behavior of different concretes. Equation (2) is used to simulate the stress–strain curve model of NWC after being exposed to high temperatures.

$$y = \frac{\sigma}{f_{c,T}} = \begin{cases} \frac{nx}{n-1+x^n}, & 0 \le x \le 1 \\ \frac{x}{\varphi(x-1)^2+x}, & x > 1 \end{cases}. \quad (2)$$

Compared with that of NWC, the rise section of ALWC and SLWC was composed of longer linear sections, and the descending section was steeper. Adding steel fiber, there was no change in the ascending part of the stress–strain curve; however, the slope at the descending part became slower. With the increase in the exposed temperature, the stress–strain curve of plain LWC and SFLWC becomes flatter, and its highest point moves down and right obviously, which was similar to NWC. The suggested equation for plain LWC and SFLWC after the elevated temperature is given as Equation (3).

$$y = \frac{\sigma}{f_{c,T}} = \begin{cases} \alpha x + (5-4\alpha)x^4 + (3\alpha-4)x^5, & 0 \le x \le 1; \\ \frac{x}{\delta(x-1)+x}, & x > 1;\ for\ plain\ LWC\ ; 25\ ^\circ\mathrm{C} \le T < 600\ ^\circ\mathrm{C} \\ \frac{x}{\varphi(x-1)^2+x}, & x > 1;\ for\ plain\ LWC; 600\ ^\circ\mathrm{C} \le T \le 800\ ^\circ\mathrm{C} \\ & x > 1;\ for\ SFLWC; 25\ ^\circ\mathrm{C} \le T \le 800\ ^\circ\mathrm{C} \end{cases}, \quad (3)$$

where $x = \varepsilon/\varepsilon_{p,T}$, and ε and σ are the compressive strain and stress of concrete, respectively; $f_{c,T}$ and $\varepsilon_{p,T}$ are the peak stress and peak strain of concrete considering the effect of temperature, respectively; $n = E_{c,T}\varepsilon_{p,T}/(E_{c,T}\varepsilon_{p,T} - f_{c,T})$ and $\alpha = E_{c,T}/E_{p,T}$; n (or α) and φ (or δ) are the shape parameters controlling the rising section and the descending section. $E_{c,T}$ and $E_{p,T}$ are initial elastic and peak secant modulus, respectively. However, $\alpha \ge 1$ can be inferred from $E_{p,T} \ge E_{c,T} > 0$. Through the regression analysis of the measured curve, Table 7 shows the values of the equation parameters.

Table 7. Regression parameters n, δ, α, and φ.

Mix	Parameters	25 °C	200 °C	400 °C	600 °C	800 °C
NWC	n	3.702	8.378	9.106	7.392	5.457
	φ	2.342	2.945	5.328	4.393	3.867
AL	α	1.000	1.045	1.000	1.205	1.243
	δ	5.155	7.701	3.820	-	-
	φ	-	-	-	4.981	10.040
SL	α	1.000	1.000	1.000	1.156	1.104
	δ	4.299	4.794	1.846	-	-
	φ	-	-	-	3.282	5.289
CFAL	α	1.065	1.186	1.026	1.270	1.364
	φ	8.657	8.548	3.423	4.731	6.809
CFSL	α	1.262	1.247	1.219	1.363	1.286
	φ	5.402	3.513	2.107	3.398	4.451
HFAL	α	1.112	1.130	1.041	1.449	1.333
	φ	4.127	2.067	3.504	4.762	5.877
HFSL	α	1.237	1.288	1.300	1.375	1.208
	φ	2.853	3.014	2.508	3.323	3.514

To verify the reliability of the model, a comparison between the theoretical and test curve is shown in Figure 15. The results showed that the theoretical curve coincides nicely with the data obtained from the test.

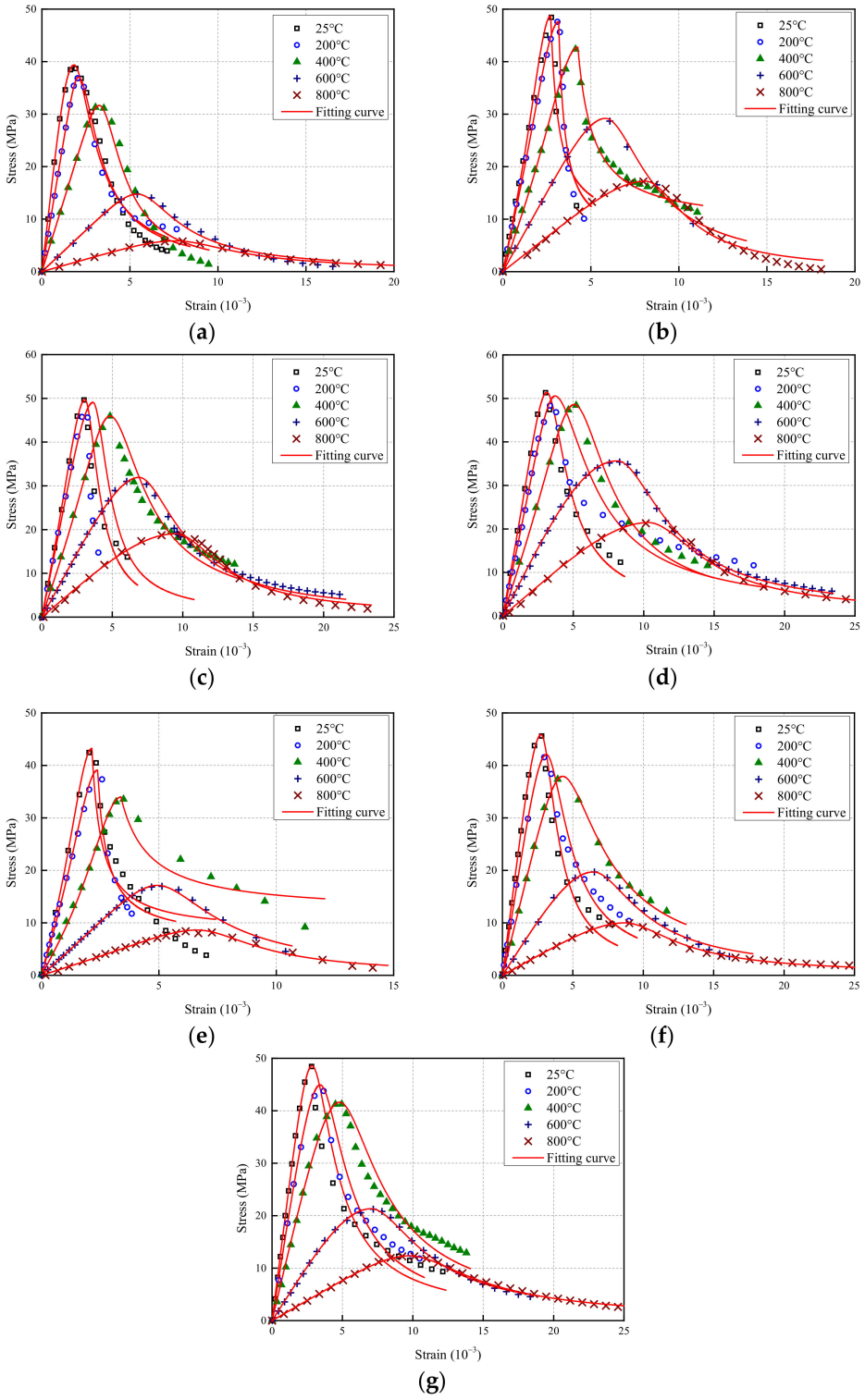

Figure 15. Comparison of the developed stress–strain relationships and experimental results: (**a**) NWC; (**b**) ALWC; (**c**) CFAL; (**d**) HFAL; (**e**) SLWC; (**f**) CFSL; (**g**) HFSL.

5. Conclusions

In this work, an experimental investigation of the residual mechanical behavior of steel fiber-reinforced LWC (SFLWC) under high temperatures has been presented. The UPVs, indirect tensile and axial compressive strengths, elastic modulus, and peak strain of these LWC specimens were evaluated. Significantly, the influences of different steel fiber types on the residual mechanical behaviors, including energy absorption capacity, elastic modulus,

and strength, have been comprehensively analyzed. The following conclusions can be drawn from the test results and analyses:

1. The evolution of the residual compressive properties of concretes after thermal treatment is mainly related to the aggregate type. It should also be noted that, in the present study, the amount of fly ash and silica fume in the concrete mixes is very small. However, further research is required to clarify the effects of mineral additives and amount of aggregate on the post-fire behavior of concrete.
2. The presence of steel fibers improved the tensile strength of both pre- and post-fire exposure. SFLWC with hooked end steel fiber lost a lesser amount of strength, which is attributed to the stronger reinforcing action to bridge the cracks. The steel fiber-reinforced ALWC had higher residual compressive and tensile strengths after heating and increased ductile performance due to the homogenous characteristics of the concrete matrix.
3. Steel fibres improve the compression absorbed energy of LWC at room temperature as well as at high temperatures. The energy absorption capacity of most concrete mixes increases for temperatures below 400 °C, but decreases above 400 °C. However, the influence of fibers on the residual elasticity modulus is minimal.
4. Simple models have been proposed to characterize the material properties as a function of temperature. The regression coefficient were all above 0.96, which indicates that the models were in good agreement with the experimental results. A numerical model is also established to predict the compressive stress–strain relationships of the heated and unheated SFLWC. The theoretical fitting curve complies well with the test results.

Author Contributions: Conceptualization, H.W., J.H., and B.C.; methodology, H.W., M.W., H.C., and B.C.; formal analysis, H.W., M.W., Y.W., and B.C.; writing—original draft preparation, H.W., M.W., H.C., B.C., and Y.W.; writing—review and editing, H.W., M.W., J.H., Y.W., and B.C.; visualization, B.C.; supervision, H.W.; project administration, H.W.; funding acquisition, H.W. All authors have read and agreed to the published version of the manuscript.

Funding: This research was funded by Guangxi University under contract no. XGZ160701, National Natural Science Foundation of China (Grant no. 51768003; 51868005), and the Science and Technology Planning Project of GuangXi Province (Grant no.2017GXNSFAA198360).

Data Availability Statement: The raw/processed data required to reproduce these findings cannot be shared at this time as the data also forms part of an ongoing study.

Conflicts of Interest: All authors declare that they have no conflict of interest.

Abbreviations

ALWC	All-lightweight concrete
CF	Crimped shape steel fiber
CFAL	All-lightweight concrete with crimped shape steel fiber
CFSL	Semi-lightweight concrete with crimped shape steel fiber
HF	Hooked end steel fiber
HFAL	All-lightweight concrete with Hooked end steel fiber
HFSL	Semi-lightweight concrete with Hooked end steel fiber
HSC	High strength concrete
LVDT	Linear Variable Differential Transformer
LWA	Lightweight aggregate
LWC	Lightweight concrete
MLWC	Multi-walled carbon nanotubes reinforced LWC
NWC	Normal-weight concrete
RPC	Reactive powder concrete
SCC	Self-consolidating concrete
SCC-S	Steel fiber-reinforced self-consolidating concrete
SFLWC	Steel fiber-reinforced lightweight concrete
SLWC	Semi-lightweight concrete
UPV	Ultrasonic pulse velocity

References

1. Akcaozoglu, S.; Atis, C.D.; Akcaozoglu, K. An investigation on the use of shredded waste PET bottles as aggregate in lightweight concrete. *Waste Manag.* **2010**, *30*, 285–290. [CrossRef] [PubMed]
2. Heiser, M.J.; Hosny, A.; Rizkalla, S.H.; Zia, P. Bond and shear behavior of concrete beams containing lightweight synthetic particles. *ACI Struct. J.* **2011**, *108*, 698–705.
3. Cui, H.Z.; Lo, T.Y.; Memon, S.A.; Xu, W. Effect of lightweight aggregates on the mechanical properties and brittleness of lightweight aggregate concrete. *Constr. Build. Mater.* **2012**, *35*, 149–158. [CrossRef]
4. Mahmoud, H.; Payam, S.; Hilmi, B.M. Lightweight aggregate concrete fiber reinforcement—A review. *Constr. Build. Mater.* **2012**, *37*, 452–461.
5. Jisun, C.; Goangseup, Z.; Shinichi, H.; Kohei, Y.; Soye, K. Influence of fiber reinforcement on strength and toughness of all-lightweight concrete. *Constr. Build. Mater.* **2014**, *69*, 381–389.
6. Dvorkin, L.; Dvorkin, O.; Zhitkovsky, V.; Ribakov, Y. A method for optimal design of steel fiber reinforced concrete composition. *Mater. Des.* **2011**, *32*, 3254–3262. [CrossRef]
7. Gao, J.; Sun, W.; Morino, K. Mechanical properties of steel fiber-reinforced, high-strength, lightweight concrete. *Cem. Concr. Compos.* **1997**, *19*, 307–313. [CrossRef]
8. Nicolas, A.L.; Mohammad, S.; Mehrdad, M.; Parviz, S. Mechanical properties of hybrid fiber reinforced lightweight aggregate concrete made with natural pumice. *Constr. Build. Mater.* **2010**, *25*, 2458–2464.
9. Wang, H.T.; Wang, L.C. Experimental study on static and dynamic mechanical properties of steel fiber reinforced lightweight aggregate concrete. *Constr. Build. Mater.* **2013**, *38*, 1146–1151. [CrossRef]
10. Thiago, M.G.; Guilherme, C.C.; Romildo, D.T.F. Fresh and hardened-state properties of self-compacting lightweight concrete reinforced with steel fibers. *Constr. Build. Mater.* **2016**, *104*, 284–292.
11. Balendran, R.V.; Zhou, F.P.; Nadeem, A.; Leung, A.Y.T. Influence of steel fibres on strength and ductility of normal and lightweight high strength concrete. *Build. Environ.* **2002**, *37*, 1361–1367. [CrossRef]
12. Bing, C.; Juanyu, L. Properties of lightweight expanded polystyrene concrete reinforced with steel fiber. *Cem. Concr. Res.* **2003**, *34*, 1259–1263.
13. Zhao, M.; Zhao, M.; Chen, M.; Li, J.; Law, D. An experimental study on strength and toughness of steel fiber reinforced expanded-shale lightweight concrete. *Constr. Build. Mater.* **2018**, *183*, 493–501. [CrossRef]
14. Topçu, İ.B.; Canbaz, M. Effect of different fibers on the mechanical properties of concrete containing fly ash. *Constr. Build. Mater.* **2007**, *21*, 1486–1491. [CrossRef]
15. Köksal, F.; Altun, F.; Yiğit, İ.; Şahin, Y. Combined effect of silica fume and steel fiber on the mechanical properties of high strength concretes. *Constr. Build. Mater.* **2008**, *22*, 1874–1880. [CrossRef]
16. Sedat, K.L.; Leyla, T.A.; Halit, Y.A.E. Young's modulus of fiber-reinforced and polymer-modified lightweight concrete composites. *Constr. Build. Mater.* **2007**, *22*, 1019–1028.
17. Iqbal, S.; Ali, A.; Holschemacher, K.; Bier, T.A. Mechanical properties of steel fiber reinforced high strength lightweight self-compacting concrete (SHLSCC). *Constr. Build. Mater.* **2015**, *98*, 325–333. [CrossRef]
18. Li, J.; Niu, J.; Wan, C.; Liu, X.; Jin, Z. Comparison of flexural property between high performance polypropylene fiber reinforced lightweight aggregate concrete and steel fiber reinforced lightweight aggregate concrete. *Constr. Build. Mater.* **2017**, *157*, 729–736.
19. Pająk, M.; Ponikiewski, T. Flexural behavior of self-compacting concrete reinforced with different types of steel fibers. *Constr. Build. Mater.* **2013**, *47*, 397–408. [CrossRef]
20. Biao, L.; Lihua, X.; Yuchuan, S.; Yin, C.; Qi, L.; Changning, L. Effects of fiber type, volume fraction and aspect ratio on the flexural and acoustic emission behaviors of steel fiber reinforced concrete. *Constr. Build. Mater.* **2018**, *181*, 474–486.
21. Ren, G.M.; Wu, H.; Fang, Q.; Liu, J.Z. Effects of steel fiber content and type on static mechanical properties of UHPCC. *Constr. Build. Mater.* **2018**, *163*, 826–839. [CrossRef]
22. Harun, T.; Ahmet, C. Performance of lightweight concrete with silica fume after high temperature. *Constr. Build. Mater.* **2007**, *22*, 2124–2129.
23. Gyu, Y.K.; Gyeong, C.C.; Yeon, W.K.; Tae, G.L. Mechanical properties of concrete depending on cooling conditions after high temperature heating. *J. Adv. Concr. Technol.* **2014**, *12*, 82–90.
24. Saridemir, M.; Severcan, M.H.; Ciflikli, M.; Celikten, S.; Ozcan, F.; Atis, C.D. The influence of elevated temperature on strength and microstructure of high strength concrete containing ground pumice and metakaolin. *Constr. Build. Mater.* **2016**, *124*, 244–257. [CrossRef]
25. Felicetti, R.; Gambarova, P.G.; Bamonte, P. Thermal and mechanical properties of light-weight concrete exposed to high temperature. *Fire Mater.* **2012**, *3*, 200–216. [CrossRef]
26. Aslani, F.; Ma, G. Normal and high-strength lightweight self-compacting concrete incorporating perlite, scoria, and polystyrene aggregates at elevated temperatures. *J. Mater. Civ. Eng.* **2018**, *30*, 04018328. [CrossRef]
27. Khaliq, W.; Kodur, V. Thermal and mechanical properties of fiber reinforced high performance self-consolidating concrete at elevated temperatures. *Cem. Concr. Res.* **2011**, *41*, 1112–1122. [CrossRef]
28. Zheng, W.; Luo, B.; Wang, Y. Compressive and tensile properties of reactive powder concrete with steel fibres at elevated temperatures. *Constr. Build. Mater.* **2013**, *41*, 844–851. [CrossRef]
29. China, M.O.C.O. *Common Portland Concrete*; Standards Press of China: Beijing, China, 2008.

30. ASTM C143/C143M. *Test Method for Slump of Hydraulic-cement Concrete*; American Society for Testing and Materials: West Conshohocken, PA, USA, 2014.
31. TS EN 12390-7. *Testing Hardened Concrete. Part 7: Density of Hardened Concrete*; British Standards Institution: London, UK, 2000.
32. ASTM C597. *Standard Test Method for Pulse Velocity Through Concrete*; American Society for Testing and Materials: West Conshohocken, PA, USA, 2003.
33. China, M.O.C.O. *Standard for Test Method of Mechanical Properties on Ordinary Concrete*; China Architecture & Building Press: Beijing, China, 2002.
34. Tai, Y.S.; Pan, H.H.; Kung, Y.N. Mechanical properties of steel fiber reinforced reactive powder concrete following exposure to high temperature reaching 800 °C. *Nucl. Eng. Des.* **2011**, *241*, 2416–2424. [CrossRef]
35. Pliya, P.; Beaucour, A.; Noumowé, A. Contribution of cocktail of polypropylene and steel fibres in improving the behaviour of high strength concrete subjected to high temperature. *Constr. Build. Mater.* **2011**, *25*, 1926–1934. [CrossRef]
36. Sinaie, S.; Heidarpour, A.; Zhao, X.L. Effect of pre-induced cyclic damage on the mechanical properties of concrete exposed to elevated temperatures. *Constr. Build. Mater.* **2016**, *112*, 867–876. [CrossRef]
37. Xie, J.; Zhang, Z.; Lu, Z.; Sun, M. Coupling effects of silica fume and steel-fiber on the compressive behaviour of recycled aggregate concrete after exposure to elevated temperature. *Constr. Build. Mater.* **2018**, *184*, 752–764.
38. Han, B.; Xiang, T. Axial compressive stress-strain relation and Poisson effect of structural lightweight aggregate concrete. *Constr. Build. Mater.* **2017**, *146*, 338–343. [CrossRef]
39. Chang, Y.F.; Chen, Y.H.; Sheu, M.S.; Yao, G.C. Residual stress–strain relationship for concrete after exposure to high temperatures. *Cem. Concr. Res.* **2006**, *36*, 1999–2005. [CrossRef]
40. Baloch, W.L.; Khushnood, R.A.; Khaliq, W. Influence of multi-walled carbon nanotubes on the residual performance of concrete exposed to high temperatures. *Constr. Build. Mater.* **2018**, *185*, 44–56. [CrossRef]
41. EN 1992-1-2 Eurocode 2. *Design of Concrete Structures, Part 1-2: General Rules—Structural Fire Design*; British Standards Institution: London, UK, 2003.
42. Zheng, W.; Li, H.; Wang, Y. Compressive stress–strain relationship of steel fiber-reinforced reactive powder concrete after exposure to elevated temperatures. *Constr. Build. Mater.* **2012**, *35*, 931–940. [CrossRef]